Annu. Rev. Fluid Mech. 2005. 37:393–423
doi: 10.1146/annurev.fluid.37.061903.175803

GRAVITY-DRIVEN BUBBLY FLOWS

Robert F. Mudde
Kramers Laboratorium voor Fysische Technologie, Delft University of Technology, 2628 BW Delft, The Netherlands; e-mail: r.f.mudde@tnw.tudelft.nl

Key Words buoyancy, vortical structures, turbulence structure, stability, LDA, CARPT, gas lift

■ **Abstract** Gravity-driven bubbly flows are a specific class of flows, where all action is provided by gravity. An industrial example is formed by the so-called bubble column: a vertical cylinder filled with liquid through which bubbles flow that are introduced at the bottom of the cylinder. On the bubble scale, gravity gives rise to buoyancy of individual bubbles. On larger scales, gravity acts on nonuniformities in the spatial bubble distribution present in the bubbly mixture. The gravity-induced flow and flow structures can increase the inhomogeneity of the bubble distribution, leading to a turbulent flow. In this flow, specific scales are identified: a large-scale circulation with the liquid flowing upward in the center of the column and downward close to the wall. On the intermediate scale there are vortical structures; eddies of liquid, with a size on the order of the diameter of the column, that stir the liquid and radially transport the bubbles. On the small scale there is the local stirring of the bubbles. We describe the ideas developed over time and identify some open questions. We discuss the experimental findings on the turbulence generated, the stability of the flow, axial dispersion, and the similarities between bubble columns and air lifts. Especially for higher gas fractions, many questions still lack accurate answers. The lateral lift force in bubble swarms and the structure of the turbulence in the bubbly mixture are important examples of inadequately understood physical phenomena, providing many challenges for fundamental and applied research on bubbly flows.

1. INTRODUCTION

In nature, as well as man-made, processes multiphase flows are frequently found. Multiphase flows can be very complicated and may comprise various phases, e.g., gas-solid flows (dust storms in nature or pneumatic transport of solids in industry), gas-liquid flows (rain, diesel sprays, or oil/gas transport in pipe lines), liquid-liquid flows, liquid-solid flows (mud flows) or gas-liquid-solid flows. A first classification runs along the different phases involved, e.g., gas-solid versus gas-liquid. Because multiphase flows show a wide variety of geometrical distribution of the phases, each with its specific features, it is customary to subdivide the multiphase flows further into separate flow regimes. For gas-liquid systems, these are usually classified via the distribution of the phases in space. On the one extreme we have gas bubbles

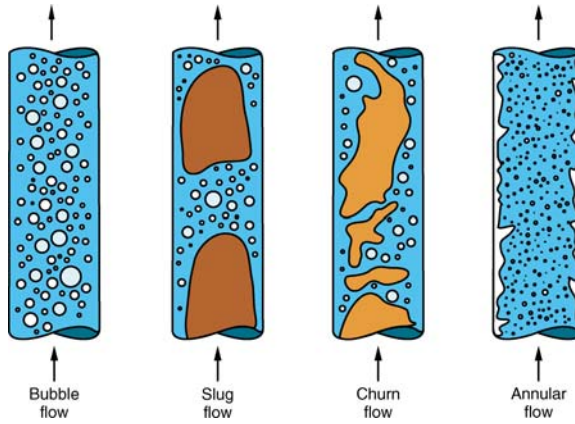

Figure 1 Flow patterns for gas-liquid flow in a vertical pipe.

dispersed in a continuous liquid phase varying via slug flow to annular flow, and on the other extreme mist flow, where droplets are dispersed in a continuous gas phase. Figure 1 illustrates this for a vertical gas-liquid flow.

At present it is impossible to treat these flows within one framework, apart of course from the notion that all gas-liquid flows are governed by two sets of Navier-Stokes equations, one for each phase. In this review we focus solely on bubbly flows driven by gravity that induces all flow. In industrial applications there are two main examples of this type of bubbly flow: the bubble column and the gas lift reactor. These reactors are popular because of the large scale that can be achieved and the absence of moving parts. The latter means low maintenance costs and relatively mild shears, which is a plus, especially in bio-applications. The drawback of these reactors is their complicated scale-up behavior.

Bubble columns are simple devices: a container filled with liquid and gassed via a sparger in the bottom or bottom region. The resulting flow depends on the gas flow rate. At low flow rates the bubbles move upward through a basically stagnant liquid. At higher gas flow rates, the bubbles tend to form clusters. Consequently, the bubble number density is no longer uniform in space and gravity reacts as locally portions of the bubbly mixture will have different densities. Liquid motion sets in at scales beyond the bubble size. This causes a further reshuffling of the bubble number density, hence hydrodynamics and gravity start to interact on global scales. Figure 2 gives an artist's impression of the development of the flow. As the figure shows, coalescence eventually sets in and there is a transition toward another flow regime. However, in large-scale equipment, the gravity-induced liquid flow is usually turbulent. The liquid turbulence causes breakup of the larger bubbles and a dynamic equilibrium sets in. Bubbly flow with a wide bubble diameter distribution is found at high-volume fractions of the gas phase. Instead of the slug flow regime, the reactor operates in the so-called churn-turbulent flow.

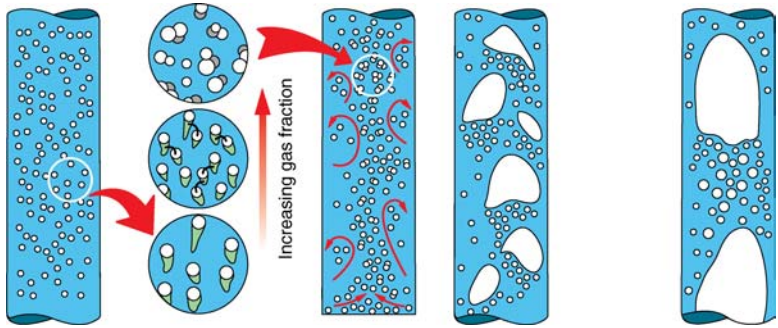

Figure 2 Transition of gravity-driven bubbly flow with increasing gas flow rate.

In this review, we concentrate on the ideas generated from experimental work. The emphasis is on the bubble column (in which the liquid phase is in batch) and on similarities with the air lift reactor. The review is organized along historical lines starting with the one-dimensional, steady-state ideas from the 1960s and 1970s and its refinements of the late 1970s and early 1980s. Next, the coherent structures put forward in the 1990s are extensively discussed. These structures shifted the attention of research to unsteady behavior and turbulence: local measurements became important. The increased insight into the structure of the flow is subsequently coupled to the macroscopic concept of axial dispersion.

In the next sections we discuss stability issues in terms of the occurrence of vortical structures and gas distribution and the importance of interaction forces, especially the transversal lift force. At the higher gas flow rates encountered in industrial applications, the bubble coalescence and breakup become important. As discussed below, the gravity-driven bubbly flows are rich in hydrodynamical structure. The interplay between gravity and (nonuniform) distribution of the bubbles results in a complex flow that has not given up all its secrets yet.

2. LARGE-SCALE CIRCULATION

The early work on the hydrodynamics of gravity-driven bubbly flows dates back to the 1960s. At that time it was observed that in bubble columns a large-scale liquid circulation is present, although the net liquid flow is zero (De Nevers 1968). The flow is upward in the central part of the column and downward close to the wall.

2.1. Rietema

To better understand this large-scale circulation, Rietema and coworkers (Rietema & Ottengraf 1970) investigated the flow in a bubble column filled with a viscous liquid (viscosity $\approx$500 mPas). Due to the high viscosity, the flow was laminar. The

bubbles were injected uniformly, but only over the inner half of the bottom of the column. Thus, a stable bubble street was formed. The gas volume fraction, α, in the bubble street was considered constant. End effects were neglected and Rietema assumed no radial pressure gradient. Rietema solved the momentum balances for the gas and liquid phase, with the constraint that the net liquid flow was zero and the assumption that the slip velocity between the bubbles and the liquid was a constant. Finally, Rietema required that the system would find the flow such that the energy dissipation was minimal. Rietema compared the analytical predictions with experimental results. The agreement is reasonable but suffers from the 1D approach: End effects are ignored and the flow is assumed to be completely developed. The predicted diameter of the bubble street is smaller than the diameter of the injector, and in experiments a continuous contraction of the bubble street is observed.

2.2. Davidson

Davidson and coworkers studied the flow in a flat, rectangular, shallow bubble column (Freedman & Davidson 1969). They used a low-viscosity oil and sparged gas over the central 44% of the bottom. Like Rietema, they observed the formation of a bubble plume that in this two-dimensional (2D) case generated two stagnant circulation cells, one at each side of the plume. The induced liquid flow is close to the bottom toward the bubbles. Hence, the bubble plume gets squeezed to a smaller region. Due to the low viscosity of the liquid, Davidson could use potential theory to describe the liquid velocity field. From his theory, Davidson could predict the properties of the plume as well as those of the liquid flow field. The agreement is reasonable.

2.3. Beek

Beek (1965) also investigated a flat, rectangular, shallow column. But in this case the bubbles were uniformly introduced over the entire bottom. Nevertheless, Beek observed the formation of plumes, separated by clear liquid circulation cells (see Figure 3). Beek observed that these circulation cells tended to have an aspect ratio

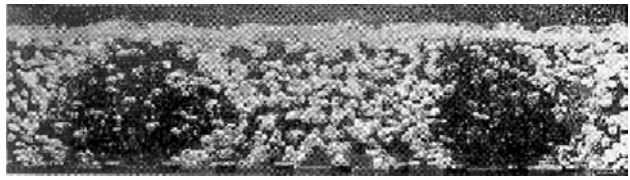

Figure 3 Spontaneous formation of plumes and clear circulation cells in an uniform gassed, flat bubble column (Beek 1965).

of 1:1. The findings show the possibility of self-organization of the bubbly flows. Even if the gas is introduced uniformly, the bubbles may form regions with higher and lower bubble number densities.

2.4. Hills

In 1974, Hills (1974) published one of the first papers on the local hydrodynamics of a bubble column. He reported radial gas fraction and averaged axial liquid velocity profiles for a 14-cm diameter air-water system. The gas fraction was measured using a resistivity probe, the liquid velocity via a modified Pitot tube. The air bubbles were introduced via the entire bottom of the column. Figure 4 summarizes the results.

As evident from the figure, the gas fraction profile is not uniform: There is a higher gas fraction in the center of the column. Gravity reacts and a large-scale liquid circulation sets in: Water flows up in the center and down along the walls. This accelerates the bubbles that flow in the center and hinders the bubbles along the wall, creating a broad residence time distribution for the bubbles. Of course, this complicates the analysis of processes carried out in the bubble column.

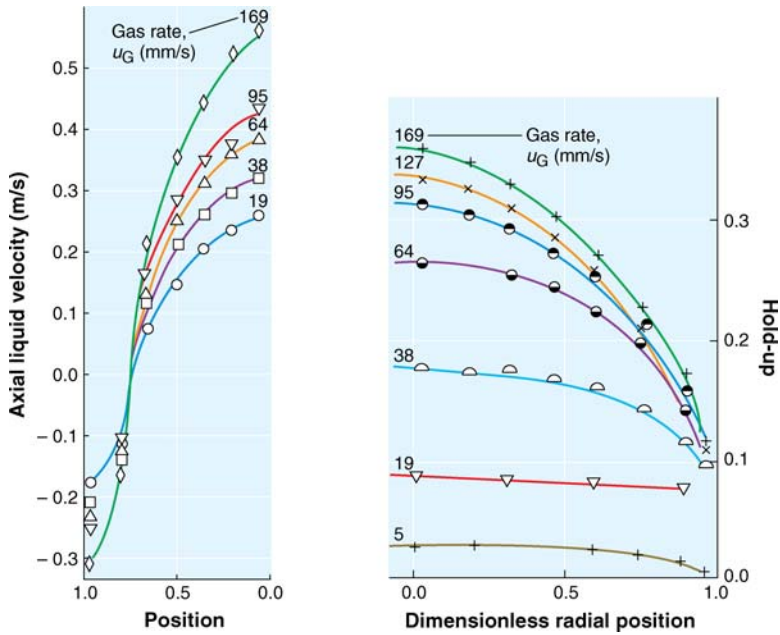

Figure 4 Radial profiles of averaged axial velocity (*left*) and gas fraction (*right*) (from Hills 1974).

2.5. Ueyama & Miyauchi

Based on a momentum balance, Ueyama & Miyauchi (1979) modeled the large-scale circulation found by Hills. Similar to Rietema, they considered the flow well developed and ignored end effects, making their model 1D. As the liquid velocity was rather high, the liquid flow was turbulent and Ueyama & Miyauchi used a turbulent viscosity. The system is closed by a prescribed gas fraction distribution:

$$\frac{\alpha}{\bar{\alpha}} = \frac{m+2}{m}\left[1 - \left(\frac{r}{R}\right)^m\right] \tag{1}$$

For the constant m, Ueyama & Miyauchi proposed a value of 2. Figure 5 shows a comparison between the radial profile of the averaged liquid velocity according to Ueyama & Miyauchi's theory and experiments available at that time.

Note that the gas fraction distribution is supposed to be known in advance. The theory does not explain why there is such a profound gas fraction profile, nor what the radial dependence should be as a function of the system parameters. In an attempt to refine the theory given above, Rice and coworkers (Geary & Rice 1992, Rice & Geary 1990) allowed the power m to vary from 5–8. In Vial et al. (2001a) this theoretical approach was confronted with experimental data of the radial profiles of the liquid velocity [measured via Laser Doppler Anemometry

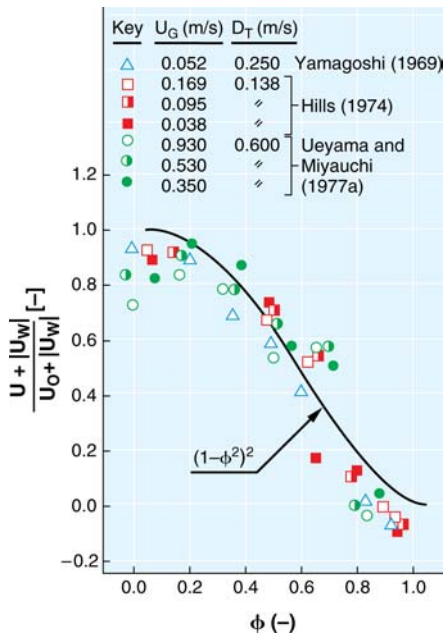

Figure 5 Radial profiles of averaged axial liquid velocity (*solid line* is the theoretical prediction). ϕ is the dimensionless radius (from Ueyama & Miyauchi 1979).

(LDA)] and of the gas fraction obtained from an optical probe. The authors concluded that good agreement could be found if a bubble-induced turbulence model was used. Furthermore, the study showed that the power m in Equation 1 varied with the sparger type used: For a single orifice m is close to 2, for a multiorifice it is about 4 for superficial gas velocities below 6 cm/s and decreases toward 2 for superficial gas velocities approaching 12 cm/s, and for a porous plate sparger it is 12 for $U_{sup} \approx 1$ cm/s and decreases to the multiorifices values at $U_{sup} \approx 6$ cm/s.

2.6. Joshi

Where Beek (1965) observed horizontally spaced, multiple circulation cells in a shallow bubble column, Joshi & Sharma (1979) argued that also in tall columns, i.e., $H/D > 3$, several circulation cells are (vertically) stacked. Whalley & Davidson (1974) showed that these cells strive for a minimal vorticity and that this drives the cells to a height-over-width ratio of 1. Therefore, Joshi & Sharma (1979) concluded that the number of cells is close to the ratio of column height over column diameter (see Figure 6).

By balancing the energy input via the gas flow to the energy dissipation, Joshi & Sharma (1979) predicted the circulation velocity of the liquid as well as the overall gas fraction. In their modeling, Joshi & Sharma (1979) could circumvent the need for a prescribed radial gas fraction profile; the model was very insensitive to the precise radial gas distribution. For air-water systems, they obtained reasonably good agreement between their model predictions and the experimental data.

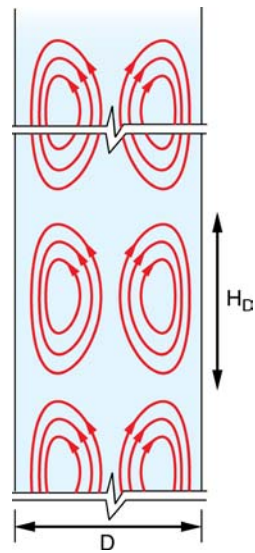

Figure 6 Multiple circulation cells, stacked vertically (Joshi & Sharma 1979).

3. COHERENT STRUCTURES

The above is a steady-state picture of the flow that concentrates on the large-scale circulation of the liquid. This is only part of the story, and in the 1990s attention shifted to smaller flow scales. The flow is much more dynamic, as is immediately apparent from visual observations. For moderate gas fractions (say around some 15%), the motion of the bubbles in the wall region alternates: part of the time the bubbles are dragged down with the liquid flow, during other times they travel upward.

3.1. Fan

For small equipment and not-too-high bubble fractions, Particle Image Velocimetry (PIV) can be used to study the flow field in bubble columns (Chen & Fan 1992). PIV measurements present fields rather than point measurements. This allowed Fan and coworkers to quantitatively study macroscopic flow structures in three-dimensional (3D) columns (Chen et al. 1994). From their studies, they concluded that the flow field in the bubble column is formed by a meandering central bubble plume and vortical structures. In a time-averaged sense, these give rise to the gross-scale circulation, with upflow in the central part of the column and downward flow in the wall region. The vortical structures represent coherent, rotating motion of patches of liquid that move through the bubble column.

Both 2D and 3D columns were studied. The former show a regular flow; the latter are rather chaotic. Figure 7 gives a schematic representation of the flow. This figure also shows the development in the ideas of the flow in the bubble columns over time.

Especially from the studies on a flat, 2D column, the occurrence and characteristics of the vortical structures have been studied in great detail. In the 2D column,

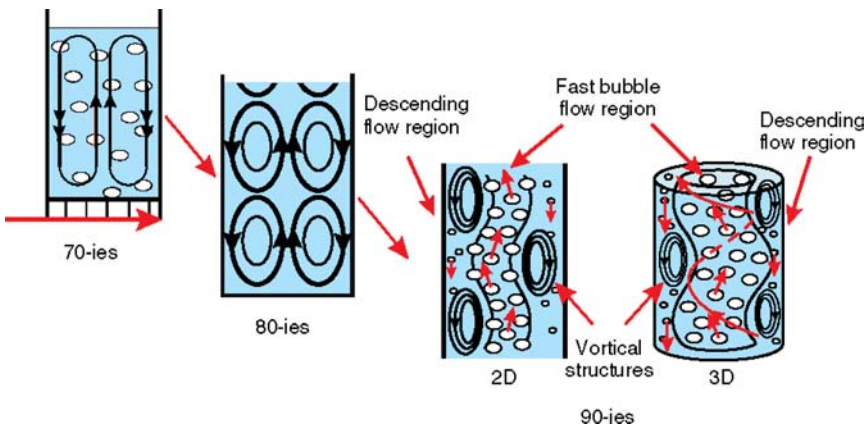

Figure 7 Schematic representation of the flow field in a bubble column (after Lin et al. 1996).

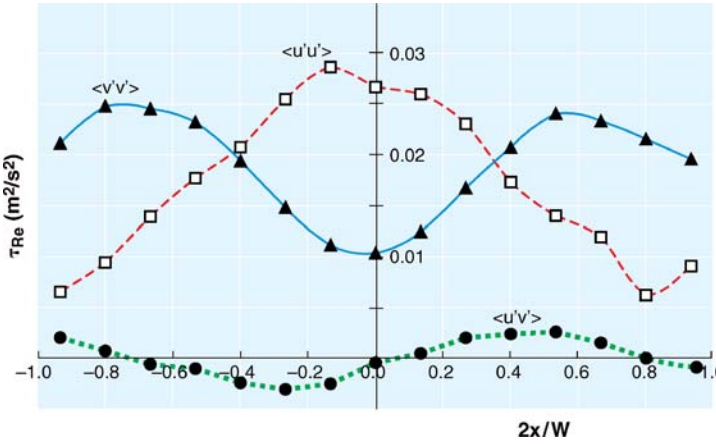

Figure 8 Reynolds stresses in the flat 2D column as a function of the horizontal coordinate, u and v are the horizontal and vertical velocity components, respectively; column width = 15 cm, superficial gas velocity = 1.0 cm/s (from Mudde et al. 1997a).

the vortical structures are formed in the upper left and right corners of the column at the free surface (Lin et al. 1996). They alternate downward: one left, one right, one left, etc. The frequency with which these structures are generated is on the order of 0.1 to 0.5 Hz.

Mudde et al. (1997a) measured the three components of the Reynolds stresses. Both normal stresses are an order of magnitude higher than the shear stress. This was also reported by Yang et al. (1993) from computer-automated radioactive particle tracking (CARPT) data in a 3D column (see below). From Figure 8, it is clear that the peak of the horizontal normal stress, $\langle u'u' \rangle$, is located at the center of the column, whereas the vertical one, $\langle v'v' \rangle$, peaks close to the wall. These findings can be understood from a kinematic picture of the motion of the vortical structures and their size. Close to the wall, the vortical structure generates a large fluctuation in the vertical velocity and only a little fluctuation in the horizontal velocity. Close to the center the opposite happens because the vortical structure spans considerably more than half of the column width. Added to that is the meandering of the central bubble plume, which generates relatively large fluctuations in the horizontal velocity in the center and only small ones in the vertical. Finally, in the 2D case the vortical structures are regular, rotating portions of liquid. Therefore, they hardly contribute to the shear stress.

The Reynolds stress has contributions from shear-induced and bubble-induced turbulence. In a first approximation, these two can be taken independently:

$$\tau_{Re} = \tau_{Re}^{SI} + \tau_{Re}^{BI}. \qquad (2)$$

The bubble-induced contribution can be estimated from potential flow around a single bubble (as the gas fraction is rather low). (See, e.g., Nigmatulin 1979):

$$\tau_{Re}^{BI} = 2 \begin{pmatrix} 4/10 & 0 & 0 \\ 0 & 3/10 & 0 \\ 0 & 0 & 3/10 \end{pmatrix} k^{BI}, \tag{3}$$

where k^{BI} is the kinetic energy density of the flow field around a bubble that can be estimated from potential theory:

$$k^{BI} = \frac{1}{2}\alpha\rho_l C_{vm} v_s^2, \tag{4}$$

with v_s the slip velocity of the bubbles and C_{vm} the virtual mass coefficient, which for bubbles of 5 mm is approximately 2 (Lance & Bataille 1991). For the data presented in Figure 8, with U_{sup} = 1.0 cm/s and $\alpha \approx 1.5\%$, the contribution to the normal stresses is on the order of $5 \cdot 10^{-3}\, m^2/s^2$. This obviously does not sufficiently explain the normal stresses reported in Figure 8.

The shear stress found by Mudde et al. (1997a), together with the velocity profile of the mean vertical velocity, suggests a Boussinesq-like relation:

$$\tau_{xy} = \rho_l \langle u'v' \rangle \approx \rho_l C \frac{d\langle v \rangle}{dx}. \tag{5}$$

From the data the authors estimated the constant C to be $5.1 \cdot 10^{-4}\,\mathrm{m}^2/\mathrm{s}$. The authors also estimated this turbulent viscosity from the $k-\epsilon$ model: $\nu_t = C_\mu \frac{k^2}{\epsilon} \approx 4.9 \cdot 10^{-4}\,\mathrm{m}^2/\mathrm{s}$, where they estimated $k = \frac{1}{2}\big(\langle u'u' \rangle + \langle v'v' \rangle\big) \sim 0.018\,\mathrm{m}^2/\mathrm{s}^2$ and the dissipations as $\epsilon = g(U_{sup} - \langle \alpha \rangle v_s)$. The agreement is rather surprising, as the use of $k-\epsilon$ could be questioned in the flat column the authors use. If the hydraulic diameter of the column ($= 2 \times$ depth $= 2.5$ cm) is used, the Reynolds number is only $5 \cdot 10^3$ based on the maximum upward liquid velocity (~ 10 cm/s).

Mudde et al. (1997a) also presented a time series of the flow. The regular passage of the vortical structures showed up as a cosine in both the horizontal and vertical velocity. Added to this cosine are the turbulent fluctuations that have an amplitude of roughly half the cosine amplitude. The contribution from the high-frequency turbulence could easily be separated from that of the low-frequency vortical structures. Thereby, the normal stresses could be separated in a contribution from the vortical structures and a remaining turbulent part. The latter resulted in flat profiles, with a magnitude about the minimum of both the total normal stresses of Figure 8. This, again, shows the significant contribution to the normal stresses by the vortical structures. But it also indicates that modeling of the turbulence in this type of bubbly flow is complicated. It is not clear whether or not the vortical structures are part of the standard turbulence cascade: In the 2D column experiments they move all the way down to the bottom, where they are squeezed. In 3D columns the picture is much more complicated, partly because of lack of information on these structures. Furthermore, the clear cut between low-frequency vortical structures and high-frequency turbulence is not present (see below). Proper model description of the underlying turbulence remains a major task for the bubbly flows.

The structures have also been observed in experiments where a bubble plume is injected in stagnant water. Especially when the sparging is not in the center of the column, there are vortical structures that move downward in combination with a meandering plume. The flow is transient, but with a clear periodic component. A good example is found in Becker et al. (1994).

3.2. Duduković

The group of Duduković developed the CARPT technique to investigate the hydrodynamics of bubbly flows (Devananthan et al. 1990; Yang et al. 1992, 1993). One, small, neutrally buoyant particle, which emits high-energy photons, is followed. The particle follows the larger eddies. By collecting the particle position over a long period of time (several hours) sufficient data are collected to estimate the ensemble-averaged velocity field and all Reynolds stresses. One of the obvious, but very important, advantages of the CARPT technique is that it works in nontransparent flows as well. This means that, where optical techniques start to fail, the higher gas fractions can be investigated.

From the data on the mean velocity, the familiar gross-scale circulation is found. The axial normal stress is roughly twice as high as the radial normal stress and almost an order of magnitude higher than the shear stresses (see Figure 9). The maximum axial normal stress is found around the point where the mean axial velocity changes sign (i.e., at $r/R \sim 0.7$).

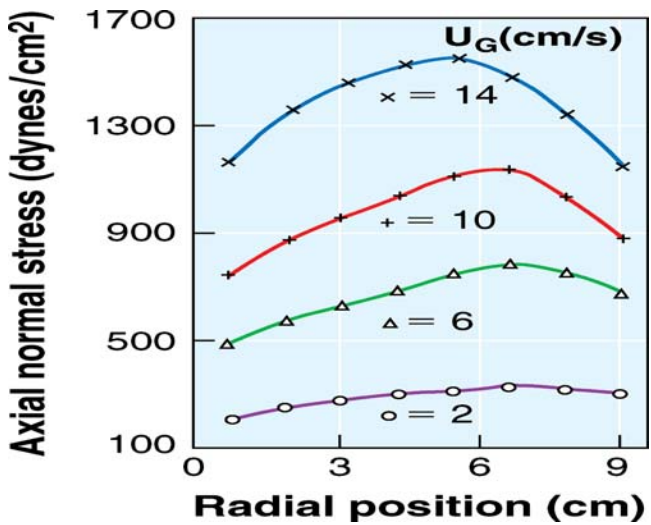

Figure 9 Reynolds stresses in a 14-cm diameter column as a function of the radial coordinate for various superficial gas velocities (from Yang et al. 1993).

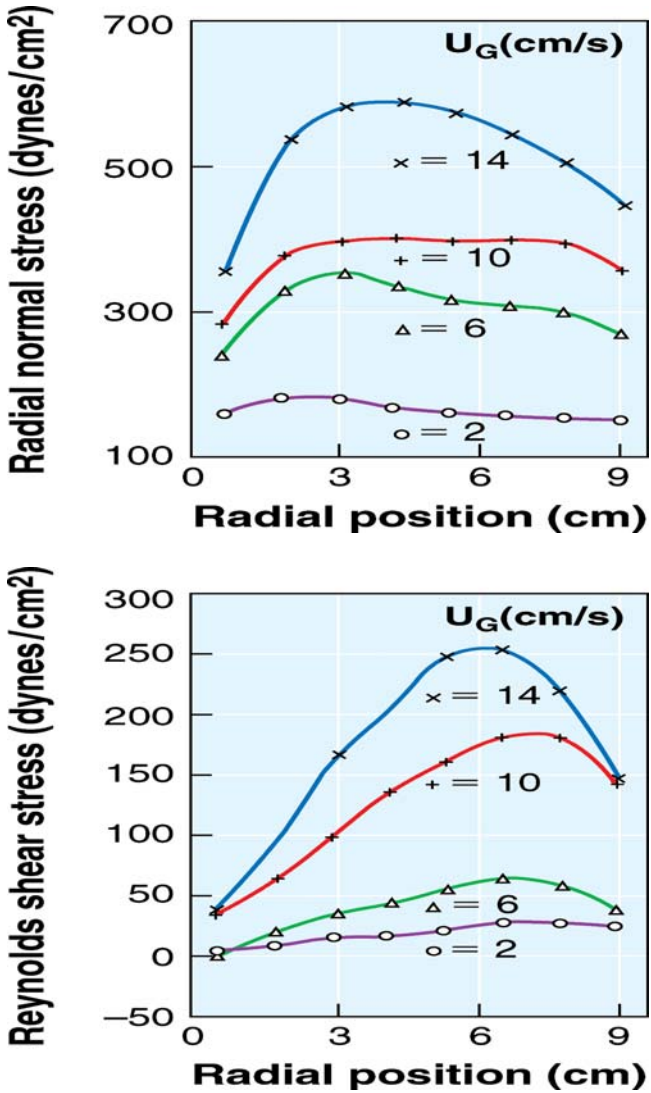

Figure 9 (*Continued*)

These findings are the 3D version of the 2D findings reported by Fan and coworkers. Clearly, the turbulence in the bubble column is anisotropic. Mudde et al. (1997b) and Vial et al. (2001a) used LDA to measure the Reynold stresses in bubble columns of various diameters and reached the same conclusion. Hence, based on these experiments, a $k - \epsilon$ approach, which is frequently tried for the flow in the bubble columns, seems inadequate. However, there are some reports

on simulations of the flow in bubble columns invoking the $k-\epsilon$ model (with two-phase modifications) that seem relatively successful. Nevertheless, the findings stress the need for an improved description of the turbulence.

Kumar et al. (1994) used gamma-densitometry tomography to measure the cross-sectional, long-time averaged gas holdup distribution in the bubble columns. As was already reported by Hills, the gas fraction profile is symmetric and peaks in the center. However, the profile is far from parabolic but follows a power law. The profile resembles that of Equation 1, and can be represented by

$$\alpha(\phi) = \bar{\alpha}\frac{m+2}{m+2-2c}(1-c\phi^m), \tag{6}$$

with $\phi = r/R$, the dimensionless radial coordinate. It deviates from the profile of Equation 1 via the constant c that allows the gas fraction to be non-zero at the wall, apart from a thin layer in which the gas fraction drops steeply to zero. Kumar et al. (1997) present more data. The parameter m decreases with both increasing column diameter and increasing superficial gas velocity and ranges from 11 to 1.6 for column diameters from 10 cm to 30 cm and U_{sup} from 2 cm/s to 8 cm/s; c ranges from 0.15 to 1. For the larger diameters, the exponent m is 2–2.5, hence the gas fraction profile is parabola-like. No further conclusions could be drawn as to the origin of the gas fraction profile, nor to the general applicability of the results. Degaleesan et al. (2001) give a more extensive survey of CARPT data for column diameters of 14 cm, 19 cm, and 44 cm. Various gas injector types were used and the superficial gas fraction ranged from 2.0 cm/s to 12.0 cm/s. Chen et al. (1999) compare CARPT and PIV data in a 10.2-cm diameter bubble column. The averaged velocities for the lower superficial gas velocity (1.9 cm/s) are in reasonable agreement but deviate for the higher superficial gas velocity (4 cm/s, $\alpha \sim 22\%$). The shear stress for the lower superficial velocity obtained from both techniques agree with one another, but for the normal stresses (i.e., axial and radial) there were differences. The same holds for the stresses measured at the higher gas velocity. This shows that we still need data sets of the Reynolds stresses that can be used as benchmark data.

3.3. Mudde & Van den Akker

Mudde & Van den Akker used LDA for the liquid velocity and optical glass fibers (Cartellier 1992, Frijlink 1987, Groen et al. 1995) for the gas fraction to investigate the properties of air-water bubble columns. Because LDA has a high spatial and good temporal resolution, it is useful to study the time series of the liquid velocity. Franz et al. (1984) were probably the first to use LDA to investigate the hydrodynamics of the bubble column. In a series of papers, Mudde & Van den Akker used LDA to study the vortical structures in 3D bubble columns. LDA measures the velocity of small particles (generally 10 μm or smaller) that are present in the flow, either as natural impurities or as added seeding particles. Because these particles are very small, they are excellent flow followers. However,

these particles are randomly distributed. Hence, LDA data comprise nonequidistant samples of the velocity, thus complicating frequency analysis. This is even more so in bubbly flows as the passing bubbles temporarily block the laser beams, thereby punching holes in the data set. However, the low-frequency part of the power spectrum is hardly disturbed and thus the temporal occurrence of the vortical structures can be found with confidence.

Mudde et al. (1997b) report LDA-experiments in a 15-cm and 23-cm air-water bubble column with the gas fraction ranging from 4% to 25%. Figure 10 shows examples of the spectra of the liquid velocity. It shows both spectra of the axial and tangential velocity. The high-frequency part seems to follow a -5/3 law. This is different from the power −8/3 reported by (Lance & Bataille 1991) found for a grid-generated turbulent bubbly flow in a 45 cm × 45 cm rectangular pipe. The low-frequency part of the APSD shows a peak at frequencies around 0.1–0.2 Hz. This reflects the passage of the vortical structures at the measuring point. A short time Fourier transform of the LDA data sets reveals that the vortical structures are not periodically passing a given point like in the 2D column discussed above. The APSD is then calculated by time windowing the data set:

$$APSD(f,t) = \left| \int v(\tau)\gamma(t-\tau)e^{-2\pi i f \tau} d\tau \right|^2 . \tag{7}$$

Figure 11 shows an example of the $APSD(f,t)$ of the axial velocity, v_{ax} (23-cm column, $U_{sup} = 4.4$ cm/s and r/ R $= 0.94$). The graph shows the time trace of v_{ax}, the APSD(f) of the total data set and, as a contour plot, the low-frequency part of the time-windowed $APSD(f,t)$. The passage of vortical structures shows up as increased activity in the contour plot at frequencies from 0–2 Hz. Clearly, the vortical structures arrive at the measuring location as separate identities with irregular spacing in time.

Becker et al. (1999) reported LDA experiments in a 29.5-cm diameter cylindrical bubble column. The column was equipped with a perforated plate sparger. These authors also reported the low-frequency oscillations, even at superficial gas velocities as low as 5 mm/s. The oscillations occurred at periods of about 20 seconds, indicating even slower oscillations than those reported by Mudde & Van den Akker (Mudde et al. 1997b). By applying chaos analysis, Becker et al. (1999) showed that the fluctuations are not periodic but have a chaotic nature (in contrast to the flat columns) in agreement with the outcome of the short time-frequency analysis discussed above.

The autocorrelation function (*ACF*) can be used to calculate the (Eulerian) integral timescale, T_I, of the flow:

$$T_I \equiv \int_0^\infty ACF(\tau)d\tau. \tag{8}$$

However, in many cases it is impractical to directly integrate the autocorrelation function. In simple turbulent flows, the autocorrelation function can be satisfactorily described by an exponential function: $ACF(t) = \exp(-t/T_I)$. Hence,

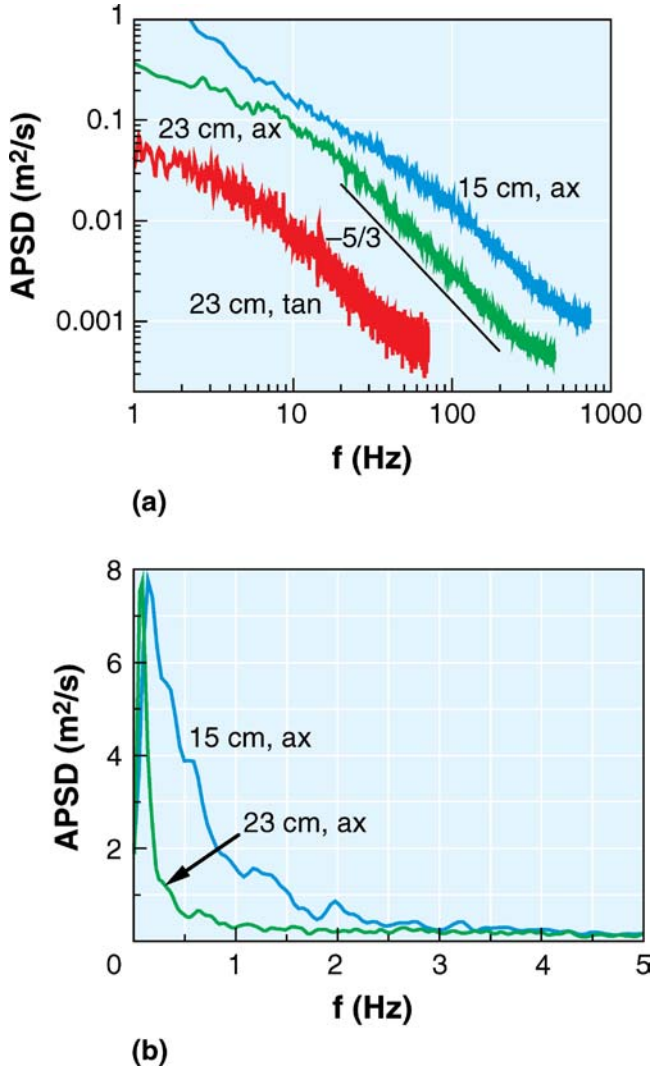

Figure 10 Auto Power Spectral Density: (*a*) high-frequency part, (*b*) low-frequency part. For the 15-cm column the superficial gas velocity is 6.7 cm/s (radial measuring position r/R = 0.94); for the 23-cm column, U_{sup} = 4.4 cm/s and r/R = 0.94 (from Mudde et al. 1997b).

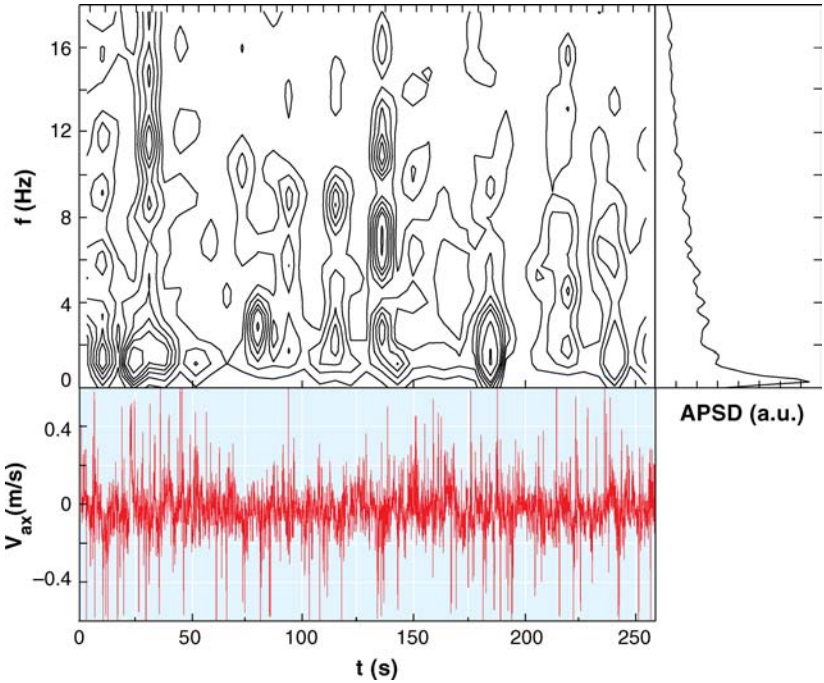

Figure 11 Short time-frequency contour plot of the axial velocity in a 23-cm column, U_{sup} = 4.4 cm/s and r/R = 0.94 (from Mudde et al. 1997b).

an exponential fit through the autocorrelation function gives an estimate of the integral timescale.

In the case of the bubble column, the vortical structures form a kind of periodicity in the flow that shows up in the autocorrelation function. The *ACF* can better be described by

$$ACF(t) = e^{-t/T_I} \cdot \cos\left(2\pi \frac{\tau}{T_{vs}}\right), \tag{9}$$

where T_{vs} is the Eulerian timescale associated with the vortical structures. In Mudde et al. (1998) the integral timescale is estimated as 0.43 s, which is similar to the Lagrangian integral timescale range of 0.4 s–0.8 s reported by Yang et al. (1993). Groen (2004) gives an overview of Eulerian timescales in three bubble columns (15-cm, 23-cm, 40-cm diameter). His results for the integral timescale and the timescale of the vortical structures are summarized in Figure 12. In Table 1 the data on the Lagrangian integral timescale from Devanathan (1991) is given.

As is seen in Figure 12, the integral timescale decreases with increasing superficial gas velocity, which is understandable because a higher superficial gas velocity means a more vigorous stirring of the fluid. The axial Eulerian integral timescale

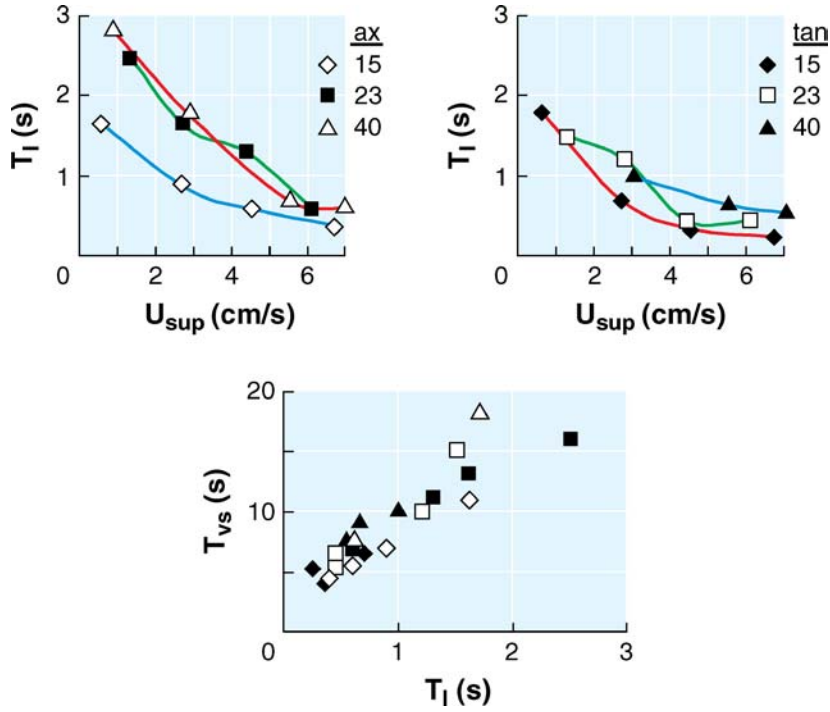

Figure 12 Dependence on the superficial gas velocity of integral timescale, T_I, and of the vortical structures, T_{vs} (from Groen 2004).

is generally longer than the radial one, and the timescale of the vortical structures shows a linear dependence on the integral timescale. The two differ by an order of magnitude.

3.4. Axial Dispersion

Due to the large-scale circulation, the vortical structures, and the liquid turbulence, bubble columns exhibit back mixing for the liquid and for the gas phase. To describe the mixing in the column, a 1D axial dispersion model is often used. A good description of the axial dispersion coefficient (E_L), for which many correlations have been developed (see, e.g., Fan 1989) is key for these models. Joshi & Sharma (1979) used the model description of the stacked multiple circulation cells to derive

$$E_L = 0.31\, D_c u_{Lc}, \tag{10}$$

with u_{Lc} the liquid circulation velocity, which follows as

$$u_{Lc} = 1.4 \left(D_c g \left[U_{sup} - \alpha u_{b\infty}\right]\right)^{1/3}, \tag{11}$$

where $u_{b\infty}$ is the terminal velocity of a single bubble.

TABLE 1 Averaged Lagrangian integral timescales (from Devanathan 1991)

Column diameter	u_{GS}	Average Lagrangian integral timescale (s)	
(*cm*)	(*cm/s*)	**Axial**	**Radial**
11.4	2.8	0.52	0.49
	6.1	0.49	0.79
19.0	2.0	0.54	0.59
	6.0	0.58	0.64
29.2	4.0	0.57	0.60
	6.0	0.56	0.62
	8.0	0.59	0.66

Groen et al. (1996) used their data from LDA experiments for the liquid velocity and glass fiber experiments for the bubble swarms on air-water bubble columns operated at relatively low superficial gas velocities (see also Groen et al. 1995). These data were used to calculate the axial dispersion coefficient based on the velocity, u_v, and size, D_v, of the dominating vortical structures:

$$E_L = u_v D_v \tag{12}$$

No additional coefficients were used and the data obtained cover the dispersion coefficients reported in reasonably well. However, as Degaleesan & Duduković (1998) pointed out, this idea does not hold for the churn-turbulent regime, where more dominant scales play a role, as Groen et al. (1995) reported.

The starting point of Degaleesan & Duduković (1998) was the steady-state, 2D convection-diffusion equation (assuming cylinder symmetry) for a scalar quantity in the liquid. This equation is, via cross-sectional area averaging, transformed in the 1D axial dispersion model. However, the axial dispersion coefficient in this model is now coupled to the underlying hydrodynamics. The dispersion coefficient has two major contributions: the dispersion caused by the axial eddy diffusivity and the so-called Taylor diffusivity that accounts for convection in the axial direction and the radial eddy diffusivity (Taylor 1954). Because the gas fraction profile is needed to evaluate the Taylor diffusivity, the data from computed tomography are also used. For the lower superficial gas velocities, the two diffusivities are about equal, but around $U_{sup} = 5\,\text{cm/s}$ the Taylor diffusivity passes through a maximum, whereas the axial eddy diffusivity continues to increase. This holds both for a column diameter of 14 cm and of 44 cm. However, the expressions for the diffusivities required some input from experimental data and, hence, there is still no general theory that can be used for scale up or different operating conditions or liquids.

4. VORTICAL STRUCTURES VERSUS UNIFORM FLOW

In all of the above, gravity acts on nonuniform distribution of the gas bubbles. However, in the models the nonuniform gas distribution is inputted via empirical relations. One important questions is: Why is the gas fraction nonuniform? As in almost all reports the gas peaks in the center, there is apparently a lateral force that drives the bubbles inward. An obvious candidate is the shear-induced lift force, which is a consequence of nonzero rotation of the liquid flow field in combination with nonzero slip between a gas bubble and the surrounding liquid:

$$\vec{F}_L = -C_L \rho_L V_b (\vec{v}_g - \vec{v}_{liq}) \times (\nabla \times \vec{v}_{liq}). \quad (13)$$

For a sphere in potential flow, the lift coefficient, C_L, has a value of 0.5. This implies that the lift force will push spherical bubbles away from the center (with the high upward velocity) toward the wall (where the liquid flows down). This is obviously in disagreement with the experimental radial bubble distribution. In a few papers, the lift force for deformable bubbles is investigated. This is, e.g., done numerically in Loth et al. (1997) and experimentally in Tomiyama et al. (2002). Both report that the lift coefficient for a certain range of bubble sizes changes sign; hence, the bubbles could migrate to the central region in the bubble column. However, note that both papers deal with isolated bubbles. Whether or not the lift coefficient follows the same size dependence for bubbles in clusters needs to be researched. It is anticipated that pressure-driven bubbly pipe flow might differ from the gravity-driven bubbly flows, as the shear might be distributed differently in both cases. The lift force is not understood to a sufficient level even for relatively simple systems. For example, Sridhar & Katz (1995) show that the lift force on small, spherical bubbles with diameters on the order of 600 μm entrained by a large vortex does not follow the usual dependence on the vorticity.

The nonuniform distribution of the bubbles could find its origin in the lift force for deformable bubbles. This suggests that the flow in the bubble columns always evolves into an unsteady flow with vortical structures and the large-scale circulation, all induced by gravity that acts on nonuniformities that arise from natural fluctuations amplified by the lift force. However, this is not true. For instance, Zahradnik et al. (1997) argued that different regimes exist: the homogeneous and heterogeneous regime with a transition regime in between. The homogeneous regime, at the lower superficial gas velocities, is characterized by a uniform bubble size and a radially uniform gas fraction. Hence, the large-scale circulation and the vortical structures are absent. The heterogeneous regime, at the higher superficial gas velocities, is characterized by a broad bubble size distribution. The gas fraction is no longer radially uniform, but has the familiar radial shape: higher in the center than in the wall region. The large-scale circulation and the vortical structures are present. The above suggests that the bubble size distribution determines the flow regime. It is true that a wide distribution of the bubbles gives

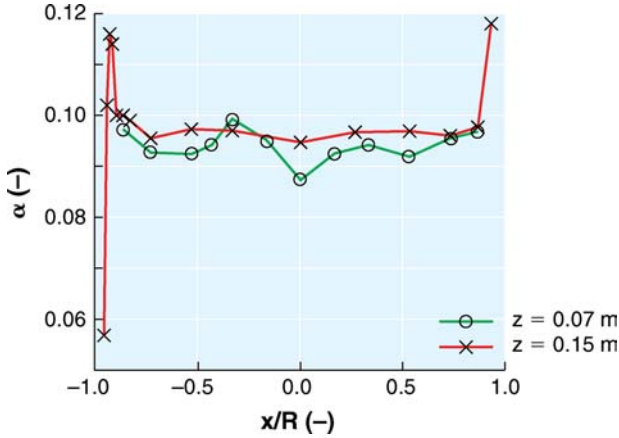

Figure 13 Radial gas fraction distribution with wall peaking, z denotes the height above the gas distributor (from Harteveld et al. 2003).

rise to the heterogeneous regime. It is not generally true that a narrow bubble size distribution implies the homogeneous regime (see, e.g., Groen et al. 1995, 1996; Mudde et al. 1997b).

Recently, Harteveld et al. (2003) reported experiments in a 15-cm diameter bubble column with gas fractions around 10%. A special sparger consisting of 561 needles was used to generate bubbles with a very narrow size distribution (~4.6-mm equivalent diameter). If the sparging of the bubbles is uniform, the gas fraction profile is very flat, with a small wall peaking (see Figure 13). The flow is very uniform and there is no large-scale liquid circulation. The turbulence levels are also low.

Next, the outer ring (of 0.75-cm thickness) of needles is switched off. A weak circulation is measured, but the flow remains stable: No large vortices are observed. If a second ring is switched off (total thickness of ungassed ring = 1.6 cm), the flow becomes strongly time dependent, with the familiar large-scale circulation and the vortical structures present. It looks similar to experiments in the same column with a porous plate at an averaged gas fraction of 8.9% (superficial gas velocity 2.0 cm/s). In more recent experiments (Harteveld et al. 2004) the flow was still stable at uniform gassing up to gas fractions of 25%. These experiments indicate that the sparger has a profound influence on the flow: The needle sparger is such that the bubbles are introduced at a fixed frequency independent of the flow properties of the bubbly mixture. Hence, there is no feedback from the flow to the sparger. Furthermore, no coalescence occurs. For the uniform sparging, or with the outer ring off, this results in a uniform flow. This is in contrast to results from computer simulations done with a single bubble size (hence no coalescence or breakup) and uniform gas injection, which report large-scale circulations. It is

clear that the modeling of the bubbly flows, even for a uniform bubble size, is still not adequate.

Garnier et al. (2002) also investigated these very uniform flows. They used a cylindrical column of 80-mm diameter. They observed uniform flow up to 40% and found very flat gas fraction profiles. They concluded that the slip velocity, U_s, of the bubbles with respect to the liquid is dictated by the cubic root of the void fraction: $(U_\infty - U_s)/U_\infty = \alpha^{1/3}$, with U_∞ the terminal rise velocity of a single bubble. The kinetic energy of the fluctuations in the liquid velocity field was proportional to the gas fraction and the slip velocity squared, thereby quantifying the stirring action of bubbles in dense swarms. The reduced freedom of the bubbles in dense swarms was also found by comparing the ratio of the liquid velocity fluctuations to those of the gas bubbles. The authors found that for the lower gas fractions (well below 10%) the ratio u'_{liq}/u'_{bub} was significant below one and approached unity for the higher gas fractions. They concluded that for the low gas fractions the bubbles have enough freedom for their wiggling motion. However, at the higher gas fractions, the bubble-bubble separation is so small that the fluctuations saturate. The freedom of the bubbles in the dense swarms is limited by their neighbors, to which they become tightly coupled via the liquid inbetween them. The behavior of bubbles in dense swarm is still a topic of research, with many questions, such as: What happens to the bubble wakes when the bubble-bubble distance is smaller than the bubble size and many bubbles are packed together? Is the vortex shedding still comparable to the case of isolated bubbles? Does the lift force change in such a case?

The stability of bubbly flows has been researched, analytically and numerically, by several researchers. Ruzicka & Thomas (2003) give a good overview of the literature. They also make a connection between thermal layers and the instabilities that occur there. The idea is that, in the homogeneous regime, the system is stable to small disturbances in the gas-fraction and the velocities. They argue that bubble-bubble interaction, i.e., hydrodynamic bubble diffusion, prevents the formation of highly buoyant bubble clusters. They also observe different types of instabilities. Although the analogy is appealing, the experiments show that at the same gas fraction both the homogeneous (i.e., without large-scale circulation) and the heterogeneous (with large-scale circulation) can be found. It might be that the start-up procedure plays an essential role here. If the start-up phase is such that a plume is formed, a mushroom type of instability is found that generates the large-scale circulation right from the start. As a consequence, the gas bubbles formed at the sparger are swept inward by the liquid circulation, thereby providing the driving force to sustain the liquid circulation. However, if a very well controlled sparger is used, this mushroom does not develop and no instability is triggered at the onset of the experiment. In between these two extremes is the possibility of a weak mushroom and hence a weak initial circulation that is too weak to counterbalance the bubble dispersion and the local driving force of the newly injected bubbles in the wall region. Once the initial stage is over and the bubble distribution is uniform, the bubbly flow turns out to be stable and small perturbations are insufficient to

generate instability. As the experiments of Harteveld et al. (2003) seem to indicate, the hydrodynamic bubble dispersion is strong enough to counteract small nonuniformities in the bubble distribution at the sparger (e.g., turning off the outer ring). The role of the sparger is probably not fully appreciated. Most spargers are fed from a single source. Consequently, the local flow through parts of the sparger is influenced by the local pressure drop over the sparger. Hydrodynamic fluctuations at the mixture side of the sparger can thus give rise to a locally fluctuating pressure drop over the sparger. This induces fluctuations in the local gas flow through the sparger into the bubbly mixture. These, in their turn, can change the local driving force for the liquid. Consequently, both positive and negative feedback are possible, not only locally but also globally. As a worst-case scenario one might wonder if much of the work done, especially at not-too-high gas flow rates, boils down to a study of the coupling between sparging and bubbly flows. To understand the gravity-driven flows better, this point deserves further attention.

Leon-Becerril et al. (2002) analytically investigated the transition from homogeneous to heterogeneous flow in bubble columns. They used a two-fluid model and studied the stability of the homogeneous regime via a linear stability analysis. In the analysis they paid special attention to the bubble shape: spherical versus oblate. The authors found a clear difference between the stability based on spherical bubbles compared to oblate ones: Oblate bubbles give rise to a much less stable flow. The critical superficial gas velocity drops from 5 cm/s for almost spherical bubbles to 3 cm/s for ellipsoidal bubbles with an aspect ratio of 2. Clearly, bubble deformation needs to be considered when dealing with the flow in bubble columns.

Lain et al. (1999) made an unexpected observation concerning the slip velocity of bubbles in a bubble column. They studied the flow properties of a bubble column at rather low gas fractions up to 3%. This low gas fraction, combined with a column diameter of 140 mm, allowed the authors to use Phase Doppler Anemometry [see also Broder & Sommerfeld (1998)], a technique that not only nonintrusively measures the particle velocity but also the size of spherical particles. Lain et al. (1999) used small bubbles to satisfy the need for spherical bubbles. In their experiment the bubble size distribution had a narrow peak around a bubble diameter of 800 μm that contained the majority of bubbles, but also a second, smaller peak with a bubble diameter of 1300 μm. Surprisingly, the slip velocity based on the mean liquid velocity and the mean bubble velocity of the bubbles (i.e., averaged over the entire bubble size distribution) was larger than the slip velocity expected from the slip velocity of the bubbles with a diameter of the 800-μm peak; the slip velocity was even higher than the slip velocity of a single, isolated bubble of 800 μm. If the Richardson & Zaki relation would have been obeyed, the slip velocity would have been slightly lower than the single bubble slip velocity. The authors point out that the observed increased slip velocity is a consequence of the interaction between the bubbles and the turbulence that causes a drag reduction. The larger bubbles were driving the flow, dragging the smaller ones via a hydrodynamic interaction. This analysis shows that there is still more to learn about hydrodynamic forces.

5. INDUSTRIAL GAS FLOW RATES

In most industrial applications, the gas flow rate is high and the system is in the heterogeneous regime. The spargers used are never fancy. The flow is often referred to as churn turbulent (say, for gas fractions of 20% and higher). This refers to the rather turbulent nature and the occurrence of large bubbles in the flow: Coalescence is strong, but a dynamic equilibrium is found by bubble break up due to the turbulence. The hydrodynamics of this flow are still inadequately understood. One major problem is the lack of proper techniques to probe the bubbles. The liquid phase can be studied via the CARPT technique mentioned above, but few details about the bubble size and bubble velocity distribution are available. Indirect information is obtained from gas disengagement experiments in which the response of the system to a sudden shut off of the gas flow rate is followed. Krishna and coworkers (Krishna et al. 1994, Krishna & Ellenberger 1996) gave some attention to this regime and concluded that, roughly speaking, the bubble phase consists of two bubble classes: the small bubbles, with diameters on the order of a few millimeters, and the large bubbles, with diameters of a centimeter and higher.

The understanding of the heterogeneous regime is far from complete. New measuring techniques to probe the bubble size and velocity are needed. The large bubbles can no longer be assumed to be ellipsoidal or spherical cap-like, but most likely have distorted shapes. This complicates the interpretation of signals from, e.g., multipoint optical probes. The bubble size distribution (and connected to that the bubble velocity distribution) is of paramount importance for the industrial applications: It determines the gas-liquid interface, the residence time distribution, and the modification of the turbulence in the liquid. All of these are important once mass transfer and chemical reactions are considered, which is obviously the case in nearly all bubbly columns. Developing new experimental techniques for the heterogeneous regime that can probe the gas characteristics is a big challenge for experimentalists dealing with the bubbly flows. This is becoming one of the bottlenecks of the research because the lack of information also hampers progress in CFD of these systems. Coalescence and breakup models need guidance from experiments and simulations that invoke coalescence and breakup and, thus, different bubbles sizes, and high-quality local data on both the gas and liquid phase.

6. AIR LIFT REACTORS

Air lift reactors form a second type of bubble reactors in which the flow is completely driven by gravity. These reactors consist of two vertical pipes joined at the top and bottom. Bubbles are introduced in the bottom region of one of the pipes; they are taken out at the top via a knockout vessel. Then, because one pipe contains bubbles and the other does not, there is a density difference between the bubbly mixture in that pipe and the clear liquid in the other. Consequently, gravity

generates a circulation: The liquid flows up in the gassed pipe, called the riser, and down in the other, called the downcomer (or downer for short). Obviously, an important difference with the bubble column is the ability for the liquid to flow unidirectionally, i.e., there is no requirement of net zero flow in a cross-sectional averaged sense and, thus, reversal of flow direction does not have to occur.

Air lift reactors find applications in the chemical industry, waste water treatment, and biotechnology. Only a few studies concerning the hydrodynamics of air lift reactors exist. This is partly due to the relative good performance of 1D models based on a mechanical energy balance and a drift flux model to couple the gas and liquid phase (see, e.g., Chisti et al. 1998, Hsu & Dudukovi ć 1980, Young et al. 1991). Due to the liquid flowing in the axial direction, the back mixing in the air lift reactors is small compared to that of the bubble column. The air lift is in a first approximation in a plug flow. However, several researchers point out the possibility of circulatory motion in the riser (see, e.g., Mercer 1981), who visually observed temporarily downward motion of bubbles close to the pipe wall in the riser). Few papers deal with the local hydrodynamics of the air lift reactor. Young et al. (1991) used a hot wire to measure the liquid velocity and gamma densitometry and a resistivity probe to obtain the gas fraction distribution. They showed that the liquid axial velocity profile is much less flat than the profile of a turbulent single phase at the same Reynolds number. The radial gas fraction profile also peaks in the center. A power-law fit of the gas fraction profile of the shape of Equation 1 gave exponents ranging between 1.6 and 2.2.

In bubbly flows in pipes of small-diameter wall, peaking, rather than core peaking, has been observed (see, e.g., Serizawa et al. 1975, Wang et al. 1987). Ohnuki & Akimoto (2000) investigated the shape of the gas fraction profile in vertical pipes of larger diameter. They found that, at a given superficial liquid velocity, the transition from wall peaking to core peaking occurs at lower superficial gas velocity if the pipe diameter increases. Mudde & Saito (2001) compared the hydrodynamics of a 15-cm diameter pipe in air lift mode to that of the same pipe in bubble column mode. Note that in the air lift mode, a pump controlled the liquid flow rate. However, the applied pressure gradient was small, so the flow remained gravity-driven. In both cases, the averaged gas fraction was about 5.5%, where the superficial liquid velocity in the air lift mode was 0.175 m/s. From a force balance the ratio of the bubble forcing over the pressure gradient is found to be almost identical in both cases. Hence, there is a great similarity between the two modes. The main conclusion is that the bulk of the bubbly flow in the air lift mode is equivalent to the flow of the bulk in the bubble column mode, but it is slowly displaced upward at the superficial liquid velocity.

The similarity even held for the stresses. In Figure 14, for example, the normal axial stress is given for both modes. In the same graph the normal axial stress for single-phase flow in the same pipe at a superficial liquid velocity of 0.175 m/s is drawn. The bubbly stresses are of the same order, whereas the single-phase stress is at least an order of magnitude lower. Furthermore, the difference between the bubbly normal stresses of both modes is close to the single-phase normal stress,

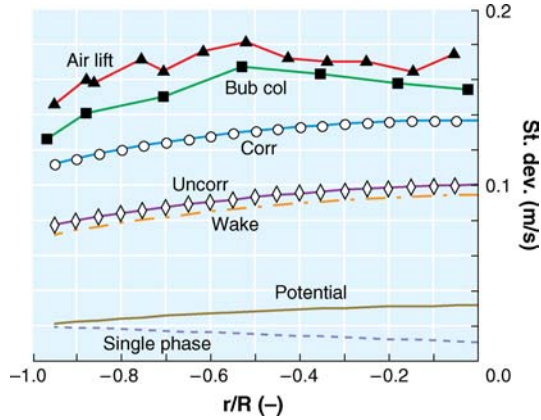

Figure 14 Standard deviation of the axial liquid velocity and the contribution of various phenomena (from Mudde & Saito 2001).

suggesting that the air lift mode is the superposition of the bubble column mode and the single-phase flow for normal stresses.

Several phenomena contribute to the stress: (*a*) potential flow around the bubbles; (*b*) bubble wakes (see, e.g., Lance & Bataille 1991); (*c*) single-phase shear, and (*d*) others, such as vortical structures. These four factors each contribute to the fluctuations in the axial velocity. Two extremes are considered: The phenomena *a* to *d* are completely uncorrelated, which gives a lower limit for the stress, and the contributions are completely correlated (at all frequencies), which gives the upper limit. Both extremes, based on phenomena *a*, *b*, and *c* are also shown in Figure 14. The stress in the bubbly flow is even higher than the completely correlated one, calling for an extra contribution like that of vortical structures.

Finally, the APSDs of the axial liquid velocity for the three flows (bubble column, air lift, and single-phase at the same liquid superficial velocity as the air lift) were compared. Again, the results show that the air lift mode and the bubble column are similar. The APSD of the air lift mode is slightly higher than that of the bubble column. This is not surprising because the same was found for the normal stress and the APSD and the normal stress are connected via Parseval's identity. The low-frequency part of the spectra revealed clearly that in both bubbly modes vortical structures are present; a short time-frequency analysis of the axial velocity in the air lift mode confirmed this.

Both the bubble columns and the air lift are basically gravity-driven. However, the stability of the flow in the air lift is increased by the net liquid upward flow. Vial et al. (2001b) reported a detailed investigation into the regime transition of both reactor types. By inspecting the Auto Correlation Function as well as the Cross Correlation Function of wall pressure fluctuations, they obtained information on

the flow and its regime. Both correlation functions were modeled using a hydrodynamical picture of the flow, similar to the modeling of the ACF of LDA data discussed above. This allows interpretation of the characteristic times in terms of a characteristic decay time and a characteristic frequency of the oscillations observed. From the cross-correlation an estimate of the vertical length scale of the fluctuations could be found. Also in this case the result was that this length scale is close to the column diameter.

A second important application of gas lifts is in the oil production industry. When an oil well ages, its down hole pressure decreases and eventually a point is reached where the down hole pressure is insufficient to keep the production of oil from the well at a reasonable level: the hydrostatic pressure of the oil (or mixture) column from the bottom hole to the oil collector or transport line is comparable to the down hole pressure available for transport. The gas lift technique helps reduce the weight of the oil column and hence enhances the production rate.

The diameters of the oil pipes involved range from 60 m to 90 mm. Based on the oil flow, the Reynolds number, in cases where gas lifting is applied, is around 10,000 (relatively low). The gas is injected from nozzles attached to the wall of the pipe. In practice, large bubbles are injected this way. Guet et al. (2003) investigated the consequences of various injection strategies for the production rate of oil; hence, on the lifting capacity of the gas introduced. They tested the nozzles presently used, a porous ring that induced small bubbles in the wall region of the tube and a vertical porous strip mounted flush in the wall that introduced small bubbles over a relatively small portion of the circumference of the pipe. Not surprisingly, they found a remarkable improvement of the gas lifting when using small bubbles rather than big ones. The small bubbles have a much lower slip velocity than the large ones. Hence, per unit volume of gas introduced, the gas fraction in the mixture is much higher and thus the reduction in weight is higher, too. The second effect is the distribution of the bubbles in the radial direction: The small bubbles are spread out rather evenly, whereas the large ones move to the center [as has been observed by many researchers (see, e.g., Serizawa et al. 1975)]. This distribution affects the radial liquid velocity, which in case of the centered large bubbles also peaks in the center, thereby increasing the absolute velocity of the bubbles even further. Finally, the large bubbles, piled up in the center, give rise to an earlier transition from the bubbly flow to slug flow. The slug flow is detrimental for the gas lifting. Hence, it is important to introduce small bubbles in such a way that they don't coalesce and are spread as uniformly as possible in the liquid. As the vertical part of flow lines in oil production can be very long, the effects of the decreasing hydrostatic pressure in the line must be considered. The bubble will expand and hence the bubble size distribution will shift to larger bubbles. Guet et al. (2003) observed that with increasing height, the radial bubble distribution shifted from uniform (or wall peaking) to core peaking. Furthermore, the transition from bubbly to slug always started when the radial bubble distribution was core peaking. A dramatic change in the gas fraction at which the transition took place could be brought about: if the initial bubble size was 13mm, the transition took

place at a gas fraction of 10%; for 7 mm bubbles, the transition occured at a gas fraction of 30%. These findings illustrate the need for a better understanding of lateral forces, coalescence, and transition to different flow regimes.

7. FINAL REMARKS

The hydrodynamics of gravity-driven bubbly flows have received a lot of attention recently. The experimental techniques have been refined and the attention has shifted from global phenomena to local phenomena. In recent decades, many features have been unraveled, e.g., the existence of the large-scale circulation and the core-peaking gas fraction profile that goes hand in hand with this circulation. The next important step was the recognition of the role of the vortical structures that provide lateral motion of the phases, enhance back mixing, and make the flow inherently unsteady. Relatively recent, renewed attention to the stability of these gravity-driven bubbly flows was initiated, both from a modeling point of view (in which connections with thermal layers and buoyancy in single-phase flows were made) and experiments (where, by careful injection of the bubbles stable, uniform flow without any vortical structures or large-scale circulation could be achieved at high gas fraction).

Modern experimental techniques have allowed the study of the turbulence structure in bubbly flows. However, it is difficult to unravel the various contributions to the liquid turbulence. Hence, we still do not have a proper description of the turbulence that can be used in numerical simulations. The turbulence is anisotropic and it is not clear to which extend the contribution from shear and from the bubbles can be added as a kind of superposition. Dedicated experiments at higher gas fraction are needed to try and find the separate contributions. The recently reported experiments with very uniform gas fraction and little induced liquid flow can play an important role here.

Despite the huge amount of literature, gravity-driven bubbly flows are not fully understood. This is partly because of the difficulties encountered in carrying out the proper experiments in bubbly flows of high gas fraction. The powerful laser-based techniques then fail. The liquid can only be probed for hydrodynamic information by hot-wires or via nuclear techniques [a radioactive particle or X-ray absorbers, as were recently employed by Seeger et al. (2001), who turned their technique into a kind of PIV]. The bubble phase is even more difficult to probe. For flows at low gas fractions, video techniques and various optical techniques can be used, but for the higher gas fractions the system is opaque. Hence, our understanding of dense bubble swarms is limited. The structure of the wakes of the bubbles is not adequately known in these swarms. Nor do we have experimental data on the lift force, which can play a dominating role because it is perpendicular to gravity. The experiments by Tomiyama et al. (2002) on the lift force show that this force is complicated. No equivalent experiments in dense swarms exist. Here is an important problem that needs attention from experiments, numerical simulations, and theory.

Because the bubble size and its distribution play an important role in the hydrodynamics as well as mass transfer in the gravity-driven bubbly flows, there is a need for experiments that focus on the bubble size distribution. Again, for the higher gas fractions this is a difficult problem. Currently, we lack proper experimental techniques to measure these unambiguously. This seriously hampers progress in industrial applications that are often operated in the high gas fraction regime, where coalescence and breakup are standard.

The above can be summarized in a wish list of topics that need to be studied.

- Turbulence structure: What is the structure of the liquid turbulence? How can the contributions from shear, relative bubble motion and wakes be modeled? How can we measure this in high gas fraction bubbly flows?
- Lateral forces in swarms: What is the sign of lateral forces in dense swarms, where the bubbles have lost their freedom to change shape and orientation compared to an isolated bubble?
- Stability: What determines the stability of the homogeneous flow? What are the proper criteria and how can we manipulate the flow?
- Bubble size and shape in dense swarms: What do bubbles look like in the churn-turbulent regime? What is their size? What is the experimental technique to answer this question?
- Coalescence and breakup: What do experiments reveal about coalescence and breakup in high gas fraction flows? What is the influence of the turbulence in the liquid phase and how is the turbulence influenced by the bubble size distribution? What is the proper experimental technique to find these answers?

From the experimental point of view, it is clear that the next generation techniques are required to solve these issues. Can we make smart sensors, perhaps microsize, that are just dumped into the flow, measure, and are sieved out and read? Can radiation (γ or X-ray) be pushed further to replace the optical techniques and provide the same type of information at the same accuracy? These are lots of questions and speculations that might help to keep the research on the gravity-driven bubbly flows alive and kicking.

This review deals exclusively with two-phase, gas-liquid flows. In many applications, however, three-phase gas-liquid-solid flows are encountered. The solids are frequently present in the form of small (i.e., submillimeter) particles that are used as catalysts to enhance or perform a specific chemical reaction. Due to the small size of the particles, the three-phase systems are almost always nontransparent. Consequently, experimentation is even more difficult. Therefore, the knowledge of the three-phase bubbly systems is not at the same level as that of the bubbly flows discussed here. It is easy to envision that similar phenomena will be present, but the presence of the dispersed solid phase will change the dependence of all kinds of phenomena on the operation condition with respect to the two-phase case. Because the systems are opaque, the development of new experimental techniques

will greatly increase the possibilities to study these systems that are relevant in many industrial operations.

ACKNOWLEDGMENTS

The author would like to thank his colleagues at the Kramers Laboratorium voor Fysische Technologie of Delft University of Technology, especially Harry van den Akker, with whom much of the work in Delft is done, and Ph.D. students Joost Groen and Wouter Harteveld, who carried out many of the experiments. I acknowledge Luis Portela for critically reviewing the manuscript and suggesting improvements. I would also like to thank L.-S. Fan, who brought the vortical structures and their role to my attention during a sabbatical leave at Ohio State University, and Mike Duduković, for his continuous cooperation and exchange of CARPT/LDA data over the years.

Finally, I acknowledge Delft University and FOM for their financial support.

LITERATURE CITED

Becker S, De Bie H, Sweeney J. 1999. Dynamic flow behaviour in bubble columns. *Chem. Eng. Sci.* 54(21):4929–35

Becker S, Sokolichin A, Eigenberger G. 1994. Gas-liquid flow in bubble columns and loop reactors: Part II. Comparison of detailed experiments and flow simulations. *Chem. Eng. Sci.* 49(24):5747–62

Beek WJ. 1965. Oscillations and vortices in a batch of liquid sustained by a gas flow. *Proc. Symp. Two-Phase Flow, Exeter, UK*, pp. F401–16

Bröder D, Sommerfeld M. 1998. Simultaneous measurements of continuous and dispersed phase in bubble columns by PDA. *Proc. 9th Int. Symp. Appl. Laser Tech. Fluid Mech., Lisbon, Portugal*, Vol. 2, Pap. 27.2

Cartellier A. 1992. Simultaneous void measurement, bubble velocity and size estimate using a single optical probe in gas-liquid two-phase flows. *Rev. Sci. Instrum.* 63:5442–53

Chen J, Kemoun A, Al-Dahhan MH, Dudukovic MP, Lee DJ, Fan L-S. 1999. Comparative hydrodynamics study in a bubble column using computer-automated radioactive particle tracking (CARPT)/computed tomography (CT) and particle image velocimetry (PIV). *Chem. Eng. Sci.* 54(13–14): 2199–207

Chen RC, Fan L-S. 1992. Particle image velocimetry for characterizing the flow structure in three-dimensional gas-liquid-solid fluidized beds. *Chem. Eng. Sci.* 47(13–14): 3615–22

Chen RC, Reese J, Fan L-S. 1994. Flow structure in a three-dimensional bubble column and three-phase fluidized bed. *AIChE J.* 40(7):1093–1104

Chisti MY, Halard B, Moo-Young M. 1988. Liquid circulation in airlift reactors. *Chem. Eng. Sci.* 43(3):451–57

Degaleesan S, Duduković MP. 1998. Liquid backmixing in bubble columns and the axial dispersion coefficient. *AIChE J.* 44(11):2369–78

Degaleesan S, Duduković MP, Pan Y. 2001. Experimental study of gas-induced liquid-flow structures in bubble columns. *AIChE J.* 47(9):1913–31

De Nevers N. 1968. Bubble driven fluid circulations. *AIChE J.* 14(2):222–26

Devanathan N. 1991. *Investigation of liquid hydrodynamics in bubble columns via a computer automated radioactive particle*

tracking (CARPT) facility. PhD thesis. Wash. Univ., St. Louis, MO

Devanathan N, Moslemian D, Duduković MP. 1990. Flow mapping in bubble columns using (CARPT). *Chem. Eng. Sci.* 45(8):2285–91

Fan L-S. 1989. *Gas-Liquid-Solid Engineering*. Boston: Butterworth

Franz K, Börner T, Kantorek HJ, Buchholz R. 1984. Flow structures in bubble columns. *Ger. Chem. Eng.* 7:365–74

Freedman W, Davidson JF. 1969. Hold-up and liquid circulation in bubble columns. *TransI-ChemE* 47:T251–61

Frijlink JJ. 1987. *Physical aspects of gassed suspension reactors*. PhD thesis. Delft Univ. Technol., The Netherlands

Garnier C, Lance M, Marié JL. 2002. Measurement of local flow characteristics in buoyancy-driven bubbly flow at high void fraction. *Exp. Therm. Fluid Sci.* 26:811–15

Geary NW, Rice RG. 1992. Circulation and scale-up in bubble columns. *AIChE J.* 38:76–82

Groen JS. 2004. *Scales and structures in bubbly flows*. PhD thesis. Delft Univ. Technol., The Netherlands

Groen JS, Mudde RF, Van den Akker HEA. 1995. Time dependent behaviour of the flow in a bubble column. *TransIChemE* 74(Part A):615–21

Groen JS, Oldeman RGC, Mudde RF, Van den Akker HEA. 1996. Coherent structures and axial dispersion in bubble column reactors. *Chem. Eng. Sci.* 51(10):2511–20

Guet S, Ooms G, Oliemans RVA, Mudde RF. 2003. Bubble injector effect on the gaslift efficiency. *AIChE J.* 49:2242–52

Harteveld WK, Julia JE, Mudde RF, Van den Akker HEA. 2004. Large scale vortical structures in bubbles columns for gas fractions in the range of 5%–25%. In press

Harteveld WK, Mudde RF, Van den Akker HEA. 2003. Dynamics of a bubble column: influence of gas distribution on coherent structures. *Can. J. Chem. Eng.* 81(3–4):389–94

Hills JH. 1974. Radial non-uniformity of velocity and voidage in a bubble column. *TransI ChemE* 52:1–9

Hsu YC, Duduković MP. 1980. Liquid recirculation in gas-lift reactors. In *Multiphase Transport Fundamentals, Reactor Safety, Applications,* ed. TN Veziroglu, 4:1757–75. Washington, DC: Hemisphere

Joshi JB, Sharma MM. 1979. A circulation model for bubble columns. *TransIChemE* 57:244–51

Krishna R, De Swart JWA, Hennephof DE, Ellenberger J, Hoefsloot HCJ. 1994. Influence of increased gas density on hydrodynamics of bubble-column reactors. *AIChE J.* 40:112–19

Krishna R, Ellenberger J. 1996. Gas holdup in bubble column reactors operating in the churn-turbulent regime. *AIChE J.* 42:2627–34

Kumar SB, Devanathan N, Moslemian D, Duduković MP. 1994. Effect of scale-up on liquid circulation in bubble columns. *Chem. Eng. Sci.* 49(24B):5637–52

Kumar SB, Moslemian D, Duduković MP. 1997. Gas-holdup measurements in bubble columns using computed tomography. *AIChE J.* 43:1414–25

Lain S, Bröder D, Sommerfeld M. 1999. Experimental and numerical studies of the hydrodynamcis in a bubble column. *Chem. Eng. Sci.* 54:4913–20

Lance M, Bataille J. 1991. Turbulence in the liquid phase of a uniform bubble air-water flow. *J. Fluid Mech.* 222:95–118

Leon-Becerril E, Cockx A, Liné A. 2002. Effect of bubble deformation on stabiltiy and mixing in bubble columns. *Chem. Eng. Sci.* 57:3283–97

Lin T-J, Reese J, Hong T, Fan L-S. 1996. Quantitative analysis and computation of two-dimensional bubble columns. *AIChE J.* 42(2):301–18

Loth E, Taeibi-Rahni M, Tryggvason G. 1997. Deformable bubbles in a free shear layer. *Int. J. Multiph. Flow* 23:977–1001

Mercer DG. 1981. Flow characteristics of a

pilot-scale airlift fermentor. *Biotechnol. Bioeng.* 29:988–94

Mudde RF, Lee DJ, Reese J, Fan L-S. 1997a. The role of coherent structures on the Reynolds stresses in a two-dimensional bubble column. *AIChE J.* 43(4):913–26

Mudde RF, Groen JS, Van den Akker HEA. 1997b. Liquid velocity field in a bubble column: LDA experiments. *Chem. Eng. Sci.* 52: 4217–24

Mudde RF, Groen JS, Van den Akker HEA. 1998. Application of LDA to bubbly flows. *Nucl. Eng. Des.* 184:329–38

Mudde RF, Saito T. 2001. Hydrodynamical similarities between bubble coulumn and bubbly pipe flow. *J. Fluid Mech.* 437:203–28

Nigmatulin RI. 1979. Spatial averaging in the mechanics of heterogeneous and dispersed systems. *Int. J. Multiph. Flow* 5:353–85

Ohnuki A, Akimoto H. 2000. Experimental study on transition of flow pattern and phase distribution in upward air-water two-phase flow along a vertical pipe. *Int. J. Multiph. Flow* 26:367–86

Rice RG, Geary NW. 1990. Prediction of liquid circulation in viscous bubble columns. *AIChE J.* 36:1339–48

Rietema K, Ottengraf SPP. 1970. Laminar liquid circulation and bubble street formation in a gas-liquid system. *TransIChemE* 48:T54–62

Ruzicka MC, Thomas NH. 2003. Buoyancy-driven instability of bubble layers: analogy with thermal convection. *Int. J. Multiph. Flow* 29:249–70

Seeger A, Affeld K, Goubergrits L, Kertzscher U, Wellnhofer E. 2001. X-ray based assessment of the three-dimensional velocity in the liquid phase in a bubble column. *Exp. Fluids* 31:193–201

Serizawa A, Kataoka I, Michiyoshi I. 1975. Turbulence structure of air-water bubbly flow-II. Local properties. *Int. J. Multiph. Flow* 2:235–46

Sridhar G, Katz J. 1995. Drag and lift forces on microscopic bubbles entrained by a vortex. *Phys. Fluids* 7(2):389–99

Taylor GI. 1954. The dispersion of matter in turbulent flow through a pipe. *Proc. R. Soc. London Ser. A* 223:446–68

Tomiyama A, Tamai H, Zun I, Hosokawa S. 2002. Transverse migration of single bubbles in simple shear flows. *Chem. Eng. Sci.* 57:1849–58

Ueyama K, Miyauchi T. 1979. Properties of recirculating turbulent two phase flow in gas bubble columns. *AIChE J.* 25(2):258–66

Vial C, Lainé R, Poncin S, Midoux N, Wild G. 2001a. Influence of gas distribution and regime transitions on liquid velocity and turbulence in a 3-D column. *Chem. Eng. Sci.* 56:1085–93

Vial C, Poncin S, Wild G, Midoux N. 2001b. A simple method for regime identification and flow characterisation in bubble columns and airlift reactors. *Chem. Eng. Proc.* 40:135–51

Wang SK, Lee SL, Jones OC, Lahey RT Jr. 1987. Local void fraction measuring techniques in two-phase using hot-wire anemometry. *Int. J. Multiph. Flow* 23:327–43

Whalley PB, Davidson JF. 1974. Liquid circulation in bubble columns. *Inst. Chem. Eng. (London) Symp. Ser.* 38:J5

Yang YB, Devanathan N, Duduković MP. 1992. Liquid backmixing in bubble columns. *Chem. Eng. Sci.* 47:2859–64

Yang YB, Devanathan N, Duduković MP. 1993. Liquid backmixing in bubble columns via computer-automated radioactive particle tracking (CARPT). *Exp. Fluids* 16:1–9

Young MA, Carbonell RG, Ollis DF. 1991. Airlift bioreactors: analysis of local two-phase hydrodynamics. *AIChE J.* 37(3):403–28

Zahradník J, Fialová M, Ruzicka M, Drahos J, Kastanek F, Thomas NH. 1997. Duality of the gas-liquid flow regimes in bubble column reactors. *Chem. Eng. Sci.* 52:3811–26

Annual Review of Fluid Mechanics
Volume 37, 2005

CONTENTS